Available online at www.sciencedirect.com
SCIENCE DIRECT®
Journal of Sound and Vibration 275 (2004) 1069–1083
JOURNAL OF SOUND AND VIBRATION
www.elsevier.com/locate/jsvi

# Stability analysis of a multibody system model for coupled slosh–vehicle dynamics

Chetan Nichkawde, P.M. Harish, N. Ananthkrishnan*

*Applied Nonlinear Dynamics and Chaos Lab, Department of Aerospace Engineering, Indian Institute of Technology (Bombay), Powai, Mumbai 400076, India*

Received 1 April 2003; accepted 4 July 2003

**Abstract**

The coupled slosh–vehicle dynamics of a rigid body in planar atmospheric flight carrying a sloshing liquid is considered as a multibody system with the sloshing motion modelled as a simple pendulum. The coupled, non-linear equations for the four-degree-of-freedom multibody system are derived using the method of Lagrangian dynamics. Careful non-dimensionalization reveals two crucial parameters that determine the extent of coupling between the rigid body and slosh modes, and also two important frequency parameters. Using a two-parameter continuation method, critical combinations of these four parameters for which the coupled slosh–vehicle dynamics can become unstable are computed. Results are displayed in the form of neutral stability curves (stability boundaries) in parameter space, and an analytical expression incorporating the four parameters that represents the neutral stability curves is obtained. Reduced-order linearized models and key transfer functions are derived in an effort to understand the instability phenomenon. Physically, the sloshing motion is seen to induce a static instability, sometimes called tumbling, in the vehicle pitch dynamics, depending on the slosh mass fraction and the location of the slosh pendulum hinge point above the rigid vehicle center of mass.


## 1. Introduction

Sloshing of liquid in tanks or containers is a problem of much concern in aerospace vehicles, ships, industries dealing with molten metal, road vehicles used as tankers, and in nuclear power plants. The sloshing liquid exerts forces and moments on the container walls that can cause structural damage. In aerospace vehicles, interaction of the slosh dynamics with the control system may have a direct impact on vehicle stability and performance. Hence, analysis of liquid

*Corresponding author. Tel.: +91-22-2576-7130, fax: +91-22-2572-2602.
*E-mail address:* akn@aero.iitb.ac.in (N. Ananthkrishnan).

0022-460X/$ - see front matter © 2003 Elsevier Ltd. All rights reserved.
doi:10.1016/j.jsv.2003.07.009

slosh in moving containers has been a problem of considerable interest, especially in the aerospace industry [1]. Launch vehicles and rockets usually contain significant amounts of liquid propellant and, ever since the development of large rockets in the 1960s, this has led to problems of instability arising from interaction between the propellant dynamics and the vehicle structural dynamics [2]. Liquid slosh in aircraft fuel tanks, though less significant, is still a matter for concern, especially in skewed tanks [3]. Spacecraft today tend to carry reasonably large amounts of liquid fuel for injection from low earth orbit to their final orbit, for station-keeping, and for precision attitude maneuvers. In these cases, the energy dissipation due to sloshing of liquid fuel can be an important factor affecting spacecraft performance [4]. Accurate models of liquid sloshing motion are therefore required to be able to predict the dynamics of fuel slosh and its influence on the overall dynamics of the vehicle carrying the liquid fuel. The importance of this subject can be gauged from the fact that a recent review reported 1319 references to literature on liquid sloshing dynamics [5].

One approach to modelling liquid sloshing motion is to use methods based on computational fluid dynamics, which seem especially attractive in cases of low-gravity slosh, and when dealing with sloshing fluid in containers of arbitrary shape [6]. However, given the complexity of the sloshing motion, these methods do not always yield reliable results (e.g., see Ref. [7, pp. 313–314]). The traditional approach has been to model the sloshing liquid by an equivalent mechanical model, such as an equivalent pendulum model or an equivalent mass–spring model [1,5]. When the parameters of the equivalent pendulum or mass–spring system are correctly chosen, the forces and moments predicted by the analysis of such a system will match with the actual hydrodynamic forces and moments due to sloshing motion. Determination of the parameters of the equivalent mechanical system is a difficult and tricky business that requires improved slosh rigs and advanced methods of data analysis [8]. The idea of equivalent mechanical models has been extended to modelling fuel slosh under low-gravity conditions [9,10]. Rotary sloshing motion under planar tank excitation has been described by a spherical pendulum model [11,12]. Fuel tanks undergoing rapid reorientation or large displacements can experience large-amplitude sloshing motion which cannot be well represented by linear mechanical models. Non-linear sloshing in spherical containers due to large tank displacement has been handled numerically under potential flow assumptions [13], and by constructing non-linear pendulum models with cubic stiffness [14]. There is thus a considerable body of knowledge related to modelling of the liquid slosh dynamics.

The challenge then is to be able to predict the dynamics of the coupled slosh–vehicle system and, in particular, those critical conditions under which the coupled system may encounter an instability. Unfortunately, very little work in this direction has been reported in the literature [4,15]. The obvious solution is to incorporate equivalent mechanical models for slosh into a multibody dynamics formulation for the coupled slosh–vehicle system, as suggested in Ref. [5]. Such a formulation would make it easy to include the effects of slosh in vehicle dynamics simulation programs and would also be suitable for use with standard control system design techniques. Instead, the present practice is to develop the equivalent mechanical models separately, independent of the vehicle dynamics. The slosh dynamics is then externally integrated with the vehicle dynamics program, with the coupled system appearing in the form of a feedback loop as shown in Fig. 1. The vehicle accelerations excite the slosh dynamics, and the slosh forces in turn act as one of the inputs to the vehicle dynamics simulation. The slosh dynamics block is usually assumed to be a linear system and is represented by a transfer function between the slosh

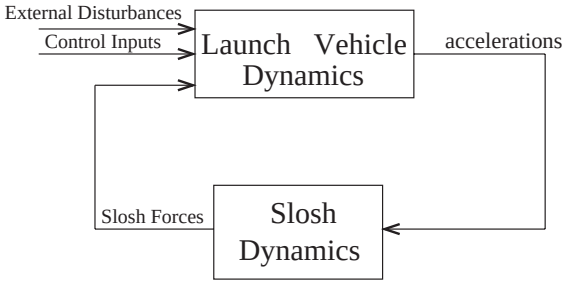


Fig. 1. Block diagram indicating how slosh models are integrated with the vehicle dynamics in the form of a feedback loop.

forces and the vehicle accelerations. Multiple slosh modes can be accommodated by introducing additional transfer functions for the higher slosh modes. However, the formulation in Fig. 1 does not account for large-amplitude sloshing motion and non-linear interactions between the slosh dynamics and the vehicle dynamics, and between the various slosh modes themselves. Non-linear interactions in dynamical systems can result in internal resonances between different parts of the system [16]. Internal resonances in systems of coupled oscillators have been known to result in instabilities [17], and such instabilities have also been observed in the flight dynamics of aerospace vehicles [18]. There is therefore much to be gained by considering the coupled slosh–vehicle dynamics as a multibody system.

The aim of the present paper is to study the coupled slosh–vehicle dynamics in terms of a multibody system model. Planar motions of a vehicle in atmospheric flight with three degrees of freedom, two translational and one rotational, are considered. A single slosh mode is considered and is modelled as a non-linear simple pendulum oscillating in the same plane as that of the vehicle motion. The four-degree-of-freedom equations of motion for the two-body system, vehicle and pendulum, are developed using the method of Lagrangian dynamics [19]. The coupled, non-linear equations of motion are suitably non-dimensionalized so as to extract the crucial parameters that determine stability. Stability boundaries in parameter space are then computed by carrying out a two-parameter continuation of the bifurcation point marking onset of instability. Details of this procedure are available in standard references [20], and they are, therefore, not elaborated on in this paper. Suffice it to say that these calculations are carried out with the complete non-linear equations of motion and do not require the slosh and vehicle dynamics to be either decoupled or linearized. The rest of the paper is devoted to understanding the instability phenomenon observed in the computations. Reduced-order models are derived to indicate that the instability arises due to coupling between the slosh dynamics and the vehicle rotational (pitch) dynamics. Analytical expressions for the curves in parameter space marking the stability boundaries are derived. In this process, transfer functions between the vehicle accelerations and the forces acting on the vehicle are obtained for the coupled slosh–vehicle system. These transfer functions are expected to be useful for control system design and parameter estimation. The multibody framework also allows, with no additional complications, consideration of multiple slosh modes, inclusion of non-linear slosh models, and more general motion of the vehicle in three-dimensional space. These issues are expected to be addressed in future work.

## 2. Coupled slosh–vehicle equations

The configuration of the coupled slosh–vehicle system under consideration is shown in Fig. 2. $m_0$ is the mass of the rigid vehicle including the mass of the fluid which does not participate in the sloshing motion, $m_0R^2$ is the rigid vehicle moment of inertia about its center of mass, $k$ is the pitch stiffness parameter, $m$ is the mass of the pendulum which represents the fraction of the fluid that is sloshing, and $l$ is its length which is a measure of the frequency of the slosh mode. The hinge point of the pendulum is located a distance $b$ from the rigid vehicle center of mass; $b$ is positive when it is as shown in Fig. 2, i.e., when the hinge point is located above the rigid vehicle center of mass. The vehicle axial and transverse displacements are represented by $x$ and $z$, respectively, while the vehicle pitch angle about its center of mass is denoted by $\theta$. The angular displacement of the pendulum from the vehicle longitudinal axis is represented by $\phi$.

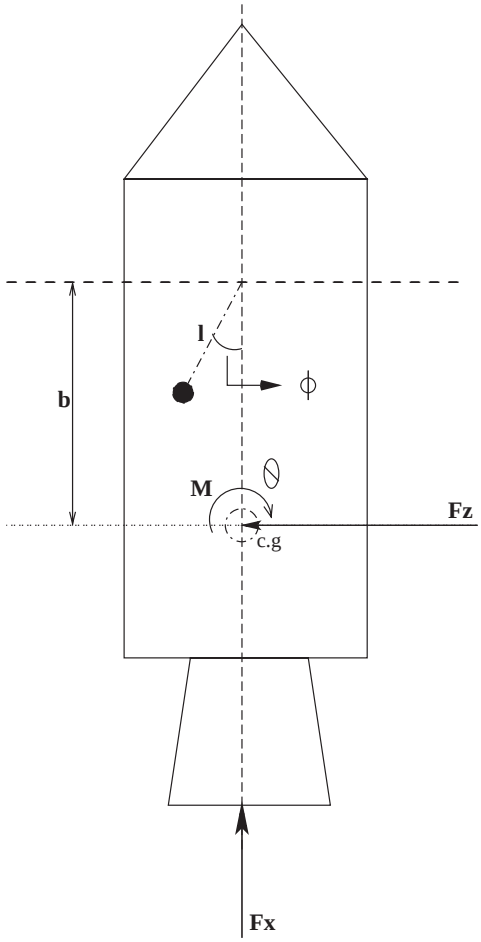


Fig. 2. Configuration of the four-degrees-of-freedom coupled slosh–vehicle system.

Let the co-ordinates of the vehicle center of mass with respect to some inertial frame of reference be $x$ and $z$. Then, the co-ordinates of the pendulum mass, $m$, will be

$$x_p = x + b\cos\theta - l\cos(\theta+\phi),$$

$$z_p = z - b\sin\theta + l\sin(\theta+\phi). \tag{1}$$

The potential energy of the system, $V$, and the kinetic energy, $T$, are then given as

$$V = m_0 g x + m g x_p + \tfrac{1}{2}k\theta^2,$$

$$T = \tfrac{1}{2}m_0(\dot{x}^2+\dot{z}^2) + \tfrac{1}{2}m_0R^2\dot{\theta}^2 + \tfrac{1}{2}m(\dot{x_p}^2+\dot{z_p}^2), \tag{2}$$

where $g$ is the acceleration due to gravity, which is assumed to be constant for simplicity, and

$$\dot{z_p} = \dot{z} - b\dot{\theta}\cos\theta + l\cos(\theta+\phi)(\dot{\theta}+\dot{\phi}),$$

$$\dot{x_p} = \dot{x} - b\dot{\theta}\sin\theta + l\sin(\theta+\phi)(\dot{\theta}+\dot{\phi}). \tag{3}$$

The Lagrangian of the system, $L = T - V$, can be written as

$$\begin{aligned} L = {} & \tfrac{1}{2}m_0(\dot{x}^2+\dot{z}^2) + \tfrac{1}{2}m_0R^2\dot{\theta}^2 + \tfrac{1}{2}m[(\dot{z} - b\dot{\theta}\cos\theta + l\cos(\theta+\phi)(\dot{\theta}+\dot{\phi}))^2 \\ & + (\dot{x} - b\dot{\theta}\sin\theta + l\sin(\theta+\phi)(\dot{\theta}+\dot{\phi}))^2] - m_0 g x \\ & - mg(x + b\cos\theta - l\cos(\theta+\phi)) - \tfrac{1}{2}k\theta^2. \end{aligned} \tag{4}$$

The equations of motion of the system can be derived using the above Lagrangian, as described in Ref. [19], as follows:

$$\begin{aligned} & (m+m_0)\ddot{z} + m\ddot{\theta}(-b\cos\theta + l\cos(\theta+\phi)) + ml\ddot{\phi}\cos(\theta+\phi) + mb\dot{\theta}^2\sin\theta \\ & - ml(\dot{\theta}+\dot{\phi})^2\sin(\theta+\phi) = F_z - c_z\dot{z}, \end{aligned} \tag{5}$$

$$\begin{aligned} & (m+m_0)\ddot{x} + m\ddot{\theta}(-b\sin\theta + l\sin(\theta+\phi)) + ml\ddot{\phi}\sin(\theta+\phi) - mb\dot{\theta}^2\cos\theta \\ & + ml(\dot{\theta}+\dot{\phi})^2\cos(\theta+\phi) + m_0 g + mg = F_x - c_x\dot{x}, \end{aligned} \tag{6}$$

$$\begin{aligned} & m_0R^2\ddot{\theta} + m\ddot{z}(-b\cos\theta + l\cos(\theta+\phi)) + m\ddot{x}(-b\sin\theta + l\sin(\theta+\phi)) \\ & + m\ddot{\theta}(b^2 + l^2 - 2bl\cos\phi) + m\ddot{\phi}(l^2 - bl\cos\phi) + 2mbl\dot{\theta}\dot{\phi}\sin\phi \\ & - mgb\sin\theta + mgl\sin(\theta+\phi) + mbl\dot{\phi}^2\sin\phi + k\theta = M - c_\theta\dot{\theta} - c_\phi\dot{\phi}, \end{aligned} \tag{7}$$

$$\begin{aligned} & ml^2\ddot{\phi} + ml\ddot{z}\cos(\theta+\phi) + ml\ddot{x}\sin(\theta+\phi) + ml\ddot{\theta}(l - b\cos\phi) - mbl\dot{\theta}^2\sin\phi \\ & + mgl\sin(\theta+\phi) = -c_\phi\dot{\phi} \end{aligned} \tag{8}$$

$c_z, c_x, c_\theta$ are the vehicle motion damping coefficients that account for any dissipative mechanism, $c_\phi$ is the slosh damping coefficient, $F_z$ and $F_x$ are the control forces (e.g., due to engine thrust) on the vehicle in the $z$ and $x$ directions, respectively, while $M$ is the resulting moment on the vehicle about its center of mass. Eqs. (5)–(8) are a more complete version of those considered in Ref. [21], where gravity has been ignored, and vehicle damping and pitch stiffness terms have been neglected. These equations are therefore valid for flight both within and outside the atmosphere, whereas the formulation in Ref. [21] is applicable only for space flight. However, in case of space

flight, the simple pendulum model for slosh may need to be replaced by a model that accounts for low-gravity effects.

### 2.1. Non-dimensionalized equations

The vehicle horizontal and vertical displacements are non-dimensionalized by the pendulum length $l$:

$$h_z = \frac{z}{l}, \quad h_x = \frac{x}{l}. \tag{9}$$

The forces and moments are non-dimensionalized by a combination of pendulum length $l$ and vehicle mass $m_0$:

$$\bar{F}_z = \frac{F_z}{m_0 l}, \quad \bar{F}_x = \frac{F_x}{m_0 l}, \quad \bar{M} = \frac{M}{m_0 l^2}. \tag{10}$$

The damping coefficients are non-dimensionalized in a manner similar to that for the forces and moments, except that the pendulum mass $m$, rather than the vehicle mass $m_0$, is used to non-dimensionalize the slosh damping coefficient $c_\phi$:

$$\bar{c}_z = \frac{c_z}{m_0}, \quad \bar{c}_x = \frac{c_x}{m_0}, \quad \bar{c}_\theta = \frac{c_\theta}{m_0 l^2}, \quad \bar{c}_\phi = \frac{c_\phi}{m l^2}. \tag{11}$$

Now, dividing the force equations (5) and (6) by $(m+m_0)l$, the moment equation (7) by $(m+m_0)l^2$, and the slosh equation (8) by $ml^2$, the non-dimensional equations are obtained as

$$\begin{aligned} &\ddot{h}_z + \varepsilon\ddot{\theta}(\cos(\theta+\phi) - \beta\cos\theta) + \varepsilon\ddot{\phi}\cos(\theta+\phi) + \varepsilon\beta\dot{\theta}^2\sin\theta \\ &\quad - \varepsilon(\dot{\theta}+\dot{\phi})^2\sin(\theta+\phi) = -\bar{c}_z(1-\varepsilon)\dot{h}_z + \bar{F}_z(1-\varepsilon), \end{aligned} \tag{12}$$

$$\begin{aligned} &\ddot{h}_x + \varepsilon\ddot{\theta}(\sin(\theta+\phi) - \beta\sin\theta) + \varepsilon\ddot{\phi}\sin(\theta+\phi) - \varepsilon\beta\dot{\theta}^2\cos\theta \\ &\quad + \varepsilon(\dot{\theta}+\dot{\phi})^2\cos(\theta+\phi) + \lambda = -\bar{c}_x(1-\varepsilon)\dot{h}_x + \bar{F}_x(1-\varepsilon), \end{aligned} \tag{13}$$

$$\begin{aligned} &\ddot{\theta}(\rho^2(1-\varepsilon) + \varepsilon\beta^2 + \varepsilon - 2\varepsilon\beta\cos\phi) + \varepsilon\ddot{\phi}(1-\beta\cos\phi) + \varepsilon\ddot{h}_z(\cos(\theta+\phi) - \beta\cos\theta) \\ &\quad + \varepsilon\ddot{h}_x(\sin(\theta+\phi) - \beta\sin\theta) + \varepsilon\beta\dot{\phi}^2\sin\phi + 2\varepsilon\beta\dot{\theta}\dot{\phi}\sin\phi - \varepsilon\lambda\beta\sin\theta \\ &\quad + \varepsilon\lambda\sin(\theta+\phi) + \bar{k}(1-\varepsilon)\theta = -\bar{c}_\theta(1-\varepsilon)\dot{\theta} - \varepsilon\bar{c}_\phi\dot{\phi} + \bar{M}(1-\varepsilon), \end{aligned} \tag{14}$$

$$\begin{aligned} &\ddot{\phi} + \ddot{\theta}(1-\beta\cos\phi) + \ddot{h}_z\cos(\theta+\phi) + \ddot{h}_x\sin(\theta+\phi) - \beta\dot{\theta}^2\sin\phi \\ &\quad + \lambda\sin(\theta+\phi) = -\bar{c}_\phi\dot{\phi}. \end{aligned} \tag{15}$$

Time is not non-dimensionalized; hence, every term in the non-dimensional equations actually has the unit $1/s^2$. The following non-dimensional parameters:

$$\varepsilon = \frac{m}{m_0+m}, \quad \rho = \frac{R}{l}, \quad \beta = \frac{b}{l} \tag{16}$$

and the following frequency parameters:

$$\lambda = \frac{g}{l}, \quad \bar{k} = \frac{k}{m_0 l^2} \tag{17}$$

appear in the above equations. The slosh mass fraction $\varepsilon$ denotes the fraction of the total vehicle mass, including the fluid mass, that participates in the sloshing motion. By definition, $\varepsilon < 1$. It may be noted that in the limit as $\varepsilon$ tends to zero, all the pendulum angular displacement terms drop out of Eqs. (12)–(14), and the vehicle dynamics equations with no slosh are correctly recovered. This implies that the slosh mass fraction $\varepsilon$ is the single most important parameter that couples the sloshing motion into the vehicle dynamics equations. Also, $\varepsilon$ does not appear in the pendulum angular motion Eq. (15), which correctly implies that the pendulum dynamics is independent of the slosh mass fraction.

When $\varepsilon$ is non-zero, the sloshing motion exerts slosh forces on the vehicle in the $x$ and $z$ directions (but no moment) at the hinge point. The slosh forces then create a moment about the rigid vehicle center of mass depending on the distance $b$ (or $\beta$ in non-dimensional form) of the pendulum hinge point from the center of mass. Thus, when $\beta = 0$, the sloshing motion does not contribute any moment to the vehicle pitch dynamics. This can be confirmed by letting $\beta$ tend to zero in the pitch dynamics equation (14). A little algebraic manipulation shows that terms satisfying the slosh equation (15) naturally drop out of the pitch dynamics equation (14), and on discarding the common factor $(1-\varepsilon)$ from the remaining terms, the vehicle pitch dynamics equation with no slosh is correctly recovered.

Besides $\varepsilon$ and $\beta$, the other parameters of interest in this study are the frequency parameters, $\lambda$ and $\bar{k}$. The inertia parameter, the non-dimensional radius of gyration, $\rho$, does not play an important role in determining the stability of the coupled slosh–vehicle system.

## 3. Stability analysis

The first step in the stability analysis of Eqs. (12)–(15) is to identify the equilibrium solutions or steady states of interest. In the most general form, the steady states are defined by the following conditions:

$$\ddot{h}_z = 0, \quad \ddot{h}_x = 0, \quad \dot{\theta} = 0, \quad \ddot{\theta} = 0, \quad \dot{\phi} = 0, \quad \ddot{\phi} = 0. \tag{18}$$

For small angles $\theta$ and $\phi$, this leads to the following conditions on the variables at the steady state, where the superscript '$*$' denotes a steady state value:

$$\begin{aligned} \dot{h}_z^* &= \bar{F}_z^* / \bar{c}_z, \\ \dot{h}_x^* &= \left( \bar{F}_x^* - \frac{\lambda}{1-\varepsilon} \right) \Big/ \bar{c}_x, \\ \theta^* &= \bar{M}^* \Big/ \left( \bar{k} - \frac{\varepsilon\lambda\beta}{1-\varepsilon} \right), \\ \phi^* &= -\bar{M}^* \Big/ \left( \bar{k} - \frac{\varepsilon\lambda\beta}{1-\varepsilon} \right). \end{aligned} \tag{19}$$

Eqs. (19) immediately reveal the condition for onset of static instability as follows:

$$\mathbf{S} = \bar{k} - \frac{\varepsilon\lambda\beta}{1-\varepsilon} = 0. \tag{20}$$

As the factor **S** approaches zero, small changes in $\bar{M}^*$ result in large changes in $\theta^*$ and $\phi^*$. In the limit when $\mathbf{S} = 0$, an infinitesimal change in $\bar{M}^*$ can cause an infinitely large change in $\theta^*$ and $\phi^*$, which signals onset of a static instability. In practice, however, the changes in $\theta^*$ and $\phi^*$ are not infinite due to non-linear effects. In any case, the static instability criterion given by the factor **S** does indicate that the vehicle pitch dynamics experiences an instability. When either $\varepsilon = 0$ or $\beta = 0$ as discussed earlier, the factor **S** reduces to simply $\bar{k} > 0$, and the pitch instability is no longer possible. Thus, it is clear that the static instability in question occurs as a result of the slosh mode coupling with the vehicle pitch dynamics. This approach to identification of instability is commonly used in the study of flight stability and control [22,23]. The following computations and analysis will confirm that it is indeed the vehicle pitch mode that loses stability when the instability condition given by the factor **S** is attained.

### 3.1. Computation of stability boundaries

By selecting the steady state value of $\bar{F}_z^*$, $\bar{F}_x^*$, and $\bar{M}^*$ in the following manner:

$$\bar{F}_z^* = 0, \quad \bar{F}_x^* = \frac{\lambda}{1-\varepsilon}, \quad \bar{M}^* = 0 \tag{21}$$

it is possible to obtain steady state values of the variables as identically zero, i.e., $\dot{h}_z^* = 0$, $\dot{h}_x^* = 0$, $\theta^* = 0$, $\phi^* = 0$, and this choice is made in the present paper for convenience. Baseline values of the various parameters are selected as follows:

$$\varepsilon = 0.3, \quad \rho = 1.1, \quad \beta = 1.5, \quad \bar{k} = 10, \quad \lambda = 19.6, \quad \bar{c}_z = \bar{c}_x = \bar{c}_\theta = \bar{c}_\phi = 0.1.$$

The above data does not pertain to any particular vehicle, but is generally representative of a launch vehicle with a partially filled cylindrical tank located at a certain distance above the vehicle center of mass. The stability of the steady state at zero is tracked with varying parameter $\varepsilon$ while keeping all other parameters fixed at their baseline values. The value of $\varepsilon$ for which a zero eigenvalue of the Jacobian matrix of the system of Eqs. (12)–(15) occurs marks the presence of a static bifurcation. For values of $\varepsilon$ below this critical value, the zero steady state is stable, whereas for values of $\varepsilon$ larger than the critical value, the zero steady state shows a static instability. Thus, the bifurcation point marks the boundary between stable and unstable behavior of the zero steady state solution with varying parameter $\varepsilon$.

With this critical value of $\varepsilon$ as a starting point, it is possible to track the bifurcation point in the $\varepsilon$–$\beta$ space using a two-parameter continuation technique. Such a computation can be carried out by using any standard continuation algorithm [20], and this gives the locus of bifurcation points in the space of two parameters, $\varepsilon$ and $\beta$. This locus of bifurcation points then marks the stability boundary in parameter space, dividing the points in $\varepsilon$–$\beta$ space into two sets, where the zero steady state solution is stable and unstable, respectively. Stability boundaries in $\varepsilon$–$\beta$ space for the coupled slosh–vehicle system given by Eqs. (12)–(15), computed in this manner, for different fixed values of the parameter $\bar{k}$, are plotted in Fig. 3. The figure is to be read as follows: For a fixed value of $\bar{k} = 10$, if $\beta$ is held at 1.5 (marked in the figure), then the coupled slosh–vehicle system will have an unstable zero steady state for $\varepsilon > 0.253$. Stability boundaries can be similarly obtained by varying any two of the parameters in the problem, and results of a computation in $\bar{k} - \lambda$ space for different fixed values of $\varepsilon$ are shown in Fig. 4. The figure suggests that for a given slosh mass

fraction and slosh frequency, the instability can be avoided by providing the vehicle with a sufficiently large pitch stiffness, and, hence, there is no necessity for actuators to directly control the sloshing motion itself. Also, the stability boundaries are independent of the slosh mode damping coefficient and are, therefore, not altered by the introduction of slosh damping augmentation devices such as baffles.

On carefully studying the curves in Figs. 3 and 4, it can be verified that they indeed satisfy the instability condition in Eq. (20), and hence the stability boundaries in these figures refer to the same phenomenon that was captured by the factor **S** in Eq. (20). The nature of the instability can be confirmed by carrying out numerical simulations for two values of the parameter $\varepsilon$: $\varepsilon = 0.3$ for which the zero steady state is unstable, and $\varepsilon = 0.1$ for which the zero steady state is stable. All other parameters are held fixed at their baseline values, and the response of the coupled slosh–vehicle system in pitch angle $\theta$ to an imperceptibly small perturbation is plotted in Fig. 5. The system clearly shows a static (divergent) instability for the larger value of $\varepsilon$ in Fig. 5 with the pitch angle $\theta$ eventually settling down to an unacceptably large value. The precise value of $\theta$ at which the simulation in Fig. 5 for $\varepsilon = 0.3$ settles down is not relevant since, under conditions of such large angular displacements, large-amplitude sloshing motion is observed, which is not well represented by the simple pendulum model considered here. Nevertheless, the qualitative phenomenon observed in the numerical simulation of Fig. 5 holds, namely, that slosh mass fractions exceeding a critical value can induce a divergent instability in vehicle pitching motion causing the vehicle to tumble [24].

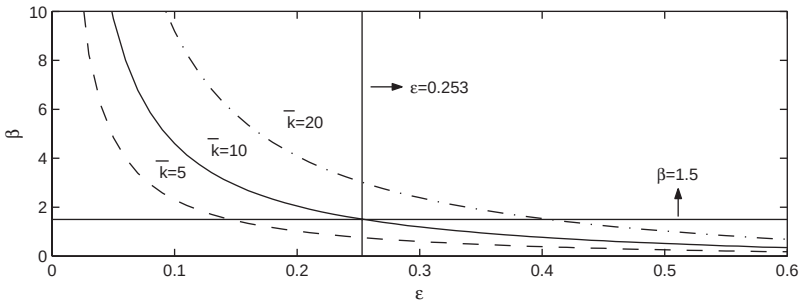


Fig. 3. Stability boundaries in $\varepsilon$–$\beta$ space for different fixed values of $\bar{k}$.

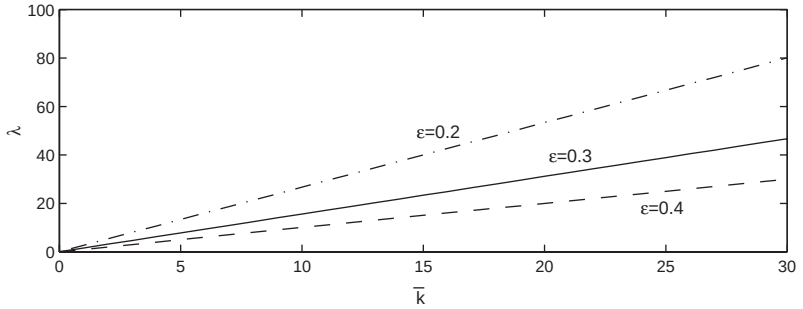


Fig. 4. Stability boundaries in $\bar{k}$–$\lambda$ space for different fixed values of $\varepsilon$.

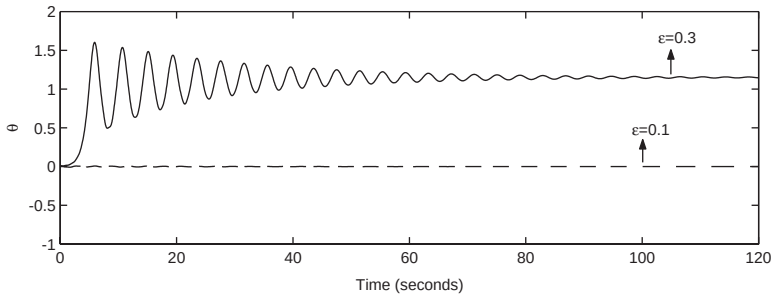


Fig. 5. Numerical simulations for two different values of $\varepsilon = 0.1, 0.3$.

## 4. Reduced-order models

To better understand the instability mechanism observed in the analysis of the four-degree-of-freedom system in the previous section, it is instructive to consider Eqs. (12)–(15) linearized about the zero steady state. The corresponding steady state values of the forces and the moment have been listed in Eq. (21). Defining small perturbations about the steady state as $\delta\dot{h}_z, \delta\dot{h}_x, \delta\theta, \delta\dot{\theta}, \delta\phi, \delta\dot{\phi}$, and small perturbations in the forces and the moment as $\delta\bar{F}_x$, $\delta\bar{F}_z$ and $\delta\bar{M}$, the linearized equations can be derived as follows:

$$\delta\ddot{h}_z + \varepsilon\delta\ddot{\theta}(1-\beta) + \varepsilon\delta\ddot{\phi} = -\bar{c}_z(1-\varepsilon)\delta\dot{h}_z + \delta\bar{F}_z(1-\varepsilon), \tag{22}$$

$$\delta\ddot{h}_x = -\bar{c}_x(1-\varepsilon)\delta\dot{h}_x + \delta\bar{F}_x(1-\varepsilon), \tag{23}$$

$$\begin{aligned}\delta\ddot{\theta}(\rho^2(1-\varepsilon) + \varepsilon(1-\beta)^2) + \varepsilon\delta\ddot{\phi}(1-\beta) + \varepsilon\delta\ddot{h}_z(1-\beta) + \varepsilon\lambda(1-\beta)\delta\theta + \varepsilon\lambda\delta\phi \\ + \bar{k}(1-\varepsilon)\delta\theta = -\bar{c}_\theta(1-\varepsilon)\delta\dot{\theta} - \varepsilon\bar{c}_\phi\delta\dot{\phi} + \delta\bar{M}(1-\varepsilon),\end{aligned} \tag{24}$$

$$\delta\ddot{\phi} + \delta\ddot{\theta}(1-\beta) + \delta\ddot{h}_z + \lambda(\delta\theta + \delta\phi) = -\bar{c}_\phi\delta\dot{\phi}. \tag{25}$$

A close look at Eqs. (22)–(25) reveals that the linearized $x$-dynamics is completely decoupled from the rest of the slosh–vehicle dynamics. It is clear from Eq. (23) that the small perturbation $x$-dynamics is itself stable as long as the $x$ damping coefficient $\bar{c}_x$ is positive. Thus, it can be safely concluded that the $x$-dynamics neither participates in nor contributes to the instability phenomenon observed in the previous section. It therefore makes sense to ignore the $x$-dynamics given by Eq. (23) and consider a reduced-order three-degree-of-freedom system consisting of Eqs. (22), (24) and (25).

### 4.1. Transfer functions

The coupling between the sloshing motion and the vehicle degrees of freedom can be studied by deriving transfer functions for the vehicle dynamics in the presence of the slosh degree of freedom. The transfer functions of interest, derived from the reduced-order system with three degrees of freedom, are the following:

$$G_z(s) = \frac{\delta\dot{h}_z(s)}{\delta\bar{F}_z(s)} = \frac{N_z}{D}, \quad G_\theta(s) = \frac{\delta\theta(s)}{\delta\bar{M}(s)} = \frac{N_\theta}{D}, \tag{26}$$

where

$$N_z = \rho^2 s^4 + \left(\bar{c}_\theta + \rho^2 \bar{c}_\phi + \frac{\varepsilon \bar{c}_\phi (1-\beta)^2}{(1-\varepsilon)}\right) s^3 + \left(\left(\bar{k} - \frac{\varepsilon\lambda\beta}{1-\varepsilon}\right) + \bar{c}_\phi \bar{c}_\theta + \lambda\left(\rho^2 + \frac{\varepsilon\beta^2}{1-\varepsilon}\right) - \frac{\varepsilon \bar{c}_\phi (1-\beta)}{1-\varepsilon}\right) s^2 + \left(\bar{c}_\phi\left(\bar{k} - \frac{\varepsilon\lambda\beta}{1-\varepsilon}\right) + \lambda \bar{c}_\theta\right) s + \lambda\left(\bar{k} - \frac{\varepsilon\lambda\beta}{1-\varepsilon}\right), \tag{27}$$

$$N_\theta = s^3 + \left(\bar{c}_z + \frac{\bar{c}_\phi}{1-\varepsilon}\right) s^2 + \left(\frac{\lambda}{1-\varepsilon} + \bar{c}_z \bar{c}_\phi\right) s + \lambda \bar{c}_z, \tag{28}$$

$$D = \rho^2 s^5 + \left(\bar{c}_\theta + \rho^2\left(\bar{c}_z + \frac{\bar{c}_\phi}{1-\varepsilon}\right) - \frac{\varepsilon \bar{c}_\phi \beta}{1-\varepsilon}(1-\beta)\right) s^4 + \left(\left(\bar{k} - \frac{\varepsilon\lambda\beta}{1-\varepsilon}\right) + \left(\rho^2 + \frac{\varepsilon\beta^2}{1-\varepsilon}\right)(\lambda + \bar{c}_z \bar{c}_\phi) + \bar{c}_\theta\left(\bar{c}_z + \frac{\bar{c}_\phi}{1-\varepsilon}\right) - \frac{\varepsilon \bar{c}_\phi \beta}{1-\varepsilon}\bar{c}_z\right) s^3 + \left(\left(\bar{c}_z + \frac{\bar{c}_\phi}{1-\varepsilon}\right)\left(\bar{k} - \frac{\varepsilon\lambda\beta}{1-\varepsilon}\right) + \lambda \bar{c}_z\left(\rho^2 + \frac{\varepsilon\beta^2}{1-\varepsilon}\right) + \bar{c}_\theta\left(\frac{\lambda}{1-\varepsilon} + \bar{c}_z \bar{c}_\phi\right)\right) s^2 + \left(\left(\frac{\lambda}{1-\varepsilon} + \bar{c}_z \bar{c}_\phi\right)\left(\bar{k} - \frac{\varepsilon\lambda\beta}{1-\varepsilon}\right) + \lambda \bar{c}_z\left(\bar{c}_\theta - \frac{\varepsilon \bar{c}_\phi \beta}{1-\varepsilon}\right)\right) s + \lambda \bar{c}_z\left(\bar{k} - \frac{\varepsilon\lambda\beta}{1-\varepsilon}\right). \tag{29}$$

For non-zero $\varepsilon$ and $\beta$, the above expressions for the vehicle transfer functions are quite complicated and capture the effect of the slosh mode coupling into the vehicle dynamics. In particular, note that the characteristic polynomial $D$ in Eq. (29) is of fifth order, and hence, the system poles, given by the roots of the characteristic polynomial, are five in number. Of these, it will be seen that the slosh dynamics always contributes a pair of complex conjugate poles, while the remaining three poles can be attributed to the vehicle dynamic modes.

Considering the limit of $\varepsilon$ tending to zero, the expressions in Eqs. (27)–(29) factor as follows:

$$N_z = (\rho^2 s^2 + \bar{c}_\theta s + \bar{k})(s^2 + \bar{c}_\phi s + \lambda),$$

$$N_\theta = (s + \bar{c}_z)(s^2 + \bar{c}_\phi s + \lambda),$$

$$D = (\rho^2 s^2 + \bar{c}_\theta s + \bar{k})(s + \bar{c}_z)(s^2 + \bar{c}_\phi s + \lambda) \tag{30}$$

which, after canceling out common factors, give the following simple expressions for the vehicle dynamics with the slosh mode decoupled:

$$G_z = \frac{1}{(s + \bar{c}_z)}, \quad G_\theta = \frac{1}{(\rho^2 s^2 + \bar{c}_\theta s + \bar{k})}. \tag{31}$$

Also, for non-zero $\varepsilon$ and in the limit as $\beta$ tends to zero, Eq. (29) factors as follows:

$$D = (\rho^2 s^2 + \bar{c}_\theta s + \bar{k})\left(s^3 + \left(\bar{c}_z + \frac{\bar{c}_\phi}{1-\varepsilon}\right) s^2 + \left(\frac{\lambda}{1-\varepsilon} + \bar{c}_z \bar{c}_\phi\right) s + \lambda \bar{c}_z\right) \tag{32}$$

and the resulting vehicle pitch transfer function $G_\theta$ takes the simple form

$$G_\theta = \frac{1}{(\rho^2 s^2 + \bar{c}_\theta s + \bar{k})} \tag{33}$$

thereby indicating that the slosh mode does not couple into the vehicle pitch dynamics when $\beta = 0$. It is also interesting to consider the case where the factor **S** in Eq. (20) is put to zero in Eqs. (27)–(29). This results in a term $s$ factoring out of the expressions for $N_z$ and $D$, but not in $N_\theta$. Then, the transfer function $G_z$ shows a cubic numerator $N_z$ and a quartic denominator $D$, after canceling out the common factor $s$, whereas the pitch transfer function $G_\theta$ retains a fifth order polynomial for the denominator $D$, but with a pole at zero due to the factor $s$. The presence of a pole at zero is an indicator of static instability, and it is possible to conclude from the above analysis that the instability occurs in the vehicle pitch dynamics given by the transfer function $G_\theta$, but not in the vehicle translational dynamics represented by $G_z$.

### 4.2. Root locus analysis

The conclusions drawn in the previous section can be confirmed by plotting the locus of the roots of the numerator and denominator polynomials in the expressions for the transfer functions in Eq. (26). For reasons of economy, root locus plots are shown here only for the case of the pitch transfer function $G_\theta(s)$. Fig. 6 shows the locus of the roots of $N_\theta$ (dashed line) and $D$ (full line) with $\varepsilon$ as the varying parameter. A similar root locus plot with $\beta$ as the varying parameter is plotted in Fig. 7. The roots in each case are plotted for the parameter varying between zero (marked on the figures by an open circle) and twice its baseline value. Both Figs. 6 and 7 show three sets of roots of the polynomial $D$ (also called poles) and two sets of roots of the polynomial $N_\theta$ (also called zeros):

1. A real pole in the left half-plane, which represents the vehicle translational motion, along with a real zero. The pole and zero are colocated when either $\varepsilon = 0$ or $\beta = 0$. With varying $\varepsilon$, both the pole and zero move to the right, but stay in the left half-plane, whereas with varying $\beta$, the pole-shifts slightly but the zero is unaffected. Thus, this root does not cross over into the right half-plane and therefore does not cause instability.

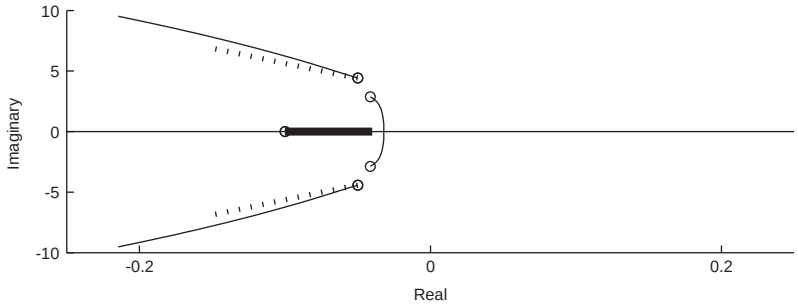


Fig. 6. Root locus of the polynomials $N_\theta$ (dashed line) and $D$ (full line) with parameter $\varepsilon$ varied from 0 (marked by open circle) to twice its baseline value. The horizontal straight line passing through 0 on the $Y$-axis is part of the root locus of $D$.

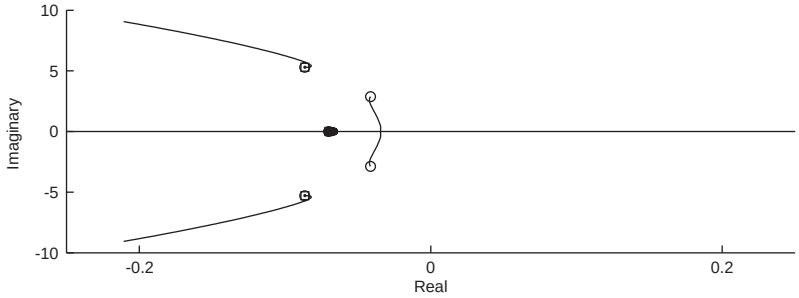


Fig. 7. Root locus of the polynomials $N_\theta$ (not a function of $\beta$) and $D$ (full line) with parameter $\beta$ varied from 0 (marked by open circle) to twice its baseline value. The horizontal straight line passing through 0 on the $Y$-axis is part of the root locus of $D$.

2. A pair of complex slosh poles along with a pair of complex zeros, both of which remain in the left half-plane when either $\varepsilon$ or $\beta$ is varied. As anticipated, for $\varepsilon = 0$ or $\beta = 0$, the slosh poles and zeros are colocated and pole-zero cancellation takes place, thus decoupling the slosh and pitch dynamics.
3. A pair of complex poles without accompanying zero, which represent the pitching motion. As either $\varepsilon$ or $\beta$ is varied, this complex conjugate pair moves towards the real axis and eventually forms two real roots. For a critical value of $\varepsilon$ or $\beta$, one of these roots crosses over into the right half-plane at the origin, causing an instability. This is the instability that was captured in the stability boundaries of Figs. 3 and 4, and by the instability condition given in Eq. (20).

The root locus analysis thus confirms that, when the sloshing motion couples into the pitch dynamics by way of a parameter such as $\varepsilon$ or $\beta$, there is a critical condition beyond which the pitch dynamics is destabilized. The critical condition for onset of instability can be easily captured by computing the stability boundaries as demonstrated in Figs. 3 and 4.

Further confirmation of the role of the pitch dynamics in the instability phenomenon due to slosh–vehicle coupling may be obtained by considering a two-degree-of-freedom system consisting of vehicle translational motion and a slosh mode, but no pitch dynamics. A system of this form is called an elliptical pendulum [25] and it has been shown that in this case the coupled slosh–vehicle dynamics does not experience an instability [26].

## 5. Conclusions

It is seen that sloshing liquid in a tank being carried by a rigid body, such as a launch vehicle, can destabilize the coupled slosh–vehicle system. The instability is more likely in case of a larger slosh mass fraction, or in case the slosh mass is located at a greater distance above the vehicle center of mass. The coupled slosh–vehicle dynamics can be modelled as a multibody system and a two-parameter continuation method can be easily used to compute the stability boundaries for this system in parameter space. Stability analysis using the continuation method provides the advantage of not requiring the multibody system equations to be either linearized or decoupled,

while, at the same time, offering some physical insight in terms of the various parameter combinations that may induce the instability. The multibody framework also allows, with no additional complications, consideration of multiple slosh modes, inclusion of non-linear slosh models, and more general motion of the vehicle in three-dimensional space. It must be mentioned that the accuracy of the results obtained obviously depends on the validity of the pendulum model used to model slosh, and on the accuracy with which estimates of the equivalent pendulum parameters are available. However, these factors are not expected to change the qualitative features of the conclusions drawn from this study.

## Appendix A. Nomenclature

| | |
|---|---|
| $b$ | distance of pendulum hinge point from rigid body center of mass |
| $c_z$ | damping coefficient for lateral translation motion |
| $c_x$ | damping coefficient for axial translation motion |
| $c_\theta$ | damping coefficient for angular motion of rigid body |
| $c_\phi$ | damping coefficient for pendulum (slosh) mass |
| $F_z$ | lateral control force on the vehicle |
| $F_x$ | axial control force on the vehicle |
| $g$ | acceleration due to gravity |
| $h_z$ | non-dimensional lateral displacement of the vehicle |
| $h_x$ | non-dimensional axial displacement of the vehicle |
| $k$ | stiffness parameter for angular (pitch) motion of rigid body |
| $L$ | Lagrangian |
| $l$ | length of pendulum |
| $M$ | external moment at rigid body center of mass |
| $m_0$ | mass of the rigid body |
| $m$ | mass of sloshing pendulum |
| $R$ | radius of gyration of the rigid body about the center of mass |
| $T$ | kinetic energy |
| $V$ | potential energy |
| $x$ | horizontal displacement of center of mass of the rigid body |
| $x_p$ | horizontal displacement of pendulum mass |
| $z$ | vertical displacement of center of mass of the rigid body |
| $z_p$ | vertical displacement of pendulum mass |
| $\beta$ | non-dimensional distance of pendulum hinge point from rigid body center of mass |
| $\phi$ | angular displacement of the pendulum |
| $\theta$ | angular displacement of the rigid body |
| $\varepsilon$ | fraction of total mass of the system participating in sloshing motion |
| $\lambda$ | natural frequency of sloshing motion |
| $\rho$ | non-dimensional radius of gyration of vehicle |

*Superscript*

| | |
|---|---|
| $\overline{()}$ | indicates non-dimensional form of quantity in $()$ |

## References


[1] H.N. Abramson, The dynamic behavior of liquids in moving containers, NASA SP 106, 1966.
[2] B.W. Oppenheim, S. Rubin, Advanced pogo stability analysis for liquid rockets, *Journal of Spacecraft and Rockets* 30 (1993) 360–373.
[3] M.J. Abzug, Fuel slosh in skewed tanks, *Journal of Guidance, Control and Dynamics* 19 (1996) 1172–1177.
[4] T. Nagata, V.J. Modi, H. Matsuo, Multibody effect on nutational dynamics of spin-stabilized satellites with fuel sloshing, *Journal of Guidance, Control and Dynamics* 21 (1998) 566–571.
[5] R.A. Ibrahim, V.N. Pilipchuk, T. Ikeda, Recent advances in liquid sloshing dynamics, *Applied Mechanics Review* 54 (2001) 133–199.
[6] R.J. Hung, Y.T. Long, Dynamical models for sloshing dynamics of helium II under low-g conditions, NASA CR 203845, 1997.
[7] J.P. Vanyo, *Rotating Fluids in Engineering and Science*, Butterworth-Heinemann, Boston, 1993.
[8] K.F. Unruh, D.D. Kana, F.T. Dodge, T.A. Fey, Digital data analysis techniques for extraction of slosh modal parameters, *Journal of Spacecraft and Rockets* 23 (1986) 171–177.
[9] F.T. Dodge, L.R. Garza, Experimental and theoretical studies of liquid sloshing at simulated low gravity, *Journal of Applied Mechanics* 34 (1967) 555–562.
[10] W.-H. Chu, Low-gravity fuel sloshing in an arbitrary axisymmetric rigid tank, *Journal of Applied Mechanics* 37 (1970) 828–837.
[11] D.D. Kana, Validated spherical pendulum model for rotary liquid slosh, *Journal of Spacecraft and Rockets* 26 (1989) 189–195.
[12] N. Ananthkrishnan, A. Verma, N.K. Sinha, S. Sudershan, Simplified spherical pendulum model for rotary liquid slosh, *Journal of the Aeronautical Society of India* 50 (1998) 129–133.
[13] J.L. Ortiz, A.A. Barhorst, Closed-form modeling of fluid–structure interaction with non-linear sloshing: potential flow, *American Institute of Aeronautics and Astronautics Journal* 35 (1997) 1510–1517.
[14] B.A. Sayar, J.R. Baumgarten, Pendulum analogy for non-linear fluid oscillations in spherical containers, *Journal of Applied Mechanics* 48 (1981) 769–772.
[15] L.D. Peterson, E.F. Crawley, R.J. Hansman, Nonlinear fluid slosh coupled to the dynamics of a spacecraft, *American Institute of Aeronautics and Astronautics Journal* 27 (1989) 1230–1240.
[16] A.H. Nayfeh, *Nonlinear Interactions*, Wiley Interscience, New York, 2000.
[17] N. Ananthkrishnan, S. Sudershan, K. Sudhakar, A. Verma, Large-amplitude limit cycles in resonantly coupled oscillators, *Journal of Sound and Vibration* 231 (2000) 1377–1382.
[18] N. Ananthkrishnan, K. Sudhakar, Characterization of periodic motions in aircraft lateral dynamics, *Journal of Guidance, Control, and Dynamics* 19 (1996) 680–686.
[19] A.L. Greensite, *Control Theory, Analysis and Design of Space Vehicle Flight Control Systems*, Spartan Books, New York, 1970.
[20] R. Seydel, *Practical Bifurcation and Stability Analysis*, 2nd Edition, Springer, New York, 1994.
[21] S. Cho, N.H. McClamroch, M. Reyhanoglu, Feedback control of a space vehicle with unactuated fuel slosh dynamics, AIAA Paper 2000-4046, *AIAA Guidance, Navigation, and Control Conference*, Denver, CO, 2000.
[22] R.C. Nelson, *Flight Stability and Automatic Control*, McGraw-Hill, Singapore, 1998.
[23] B. Etkin, L.D. Reid, *Dynamics of Flight: Stability and Control*, Wiley, New York, 1996.
[24] M.J. Sidi, *Spacecraft Dynamics and Control*, Cambridge University Press, Cambridge, 1997.
[25] Z.M. Ge, T.N. Lin, Regular and chaotic dynamic analysis and control of an elliptical pendulum on a vibrating basement, *Journal of Sound and Vibration* 230 (2000) 1045–1068.
[26] P.M. Harish, N. Ananthkrishnan, C. Nichkawde, Modeling and analysis of coupled slosh–vehicle dynamics, *Proceedings of the Second International Conference on Fluid Mechanics and Fluid Power*, Roorkee, India, 2002, pp. 305–312.